Hydrocarbon Fueled UUV Power Systems

D. H. Kiely, J. T. Moore
Applied Research Laboratory
The Pennsylvania State University
P. O. Box 30
State College, PA 16804

Abstract-**Two hydrocarbon fueled internal combustion UUV power sources incorporating a high-speed turbo-alternator are described, and their performance variation with operating depth and total energy is discussed. Turbine performance data is also discussed. These systems require only the refilling of tanks without disassembly between runs. They have overall system specific energies 3 to 4 times that of silver-zinc batteries.**

I. Introduction

The Applied Research Laboratory (ARL) at Penn State University has a long history of developing power systems for underwater vehicles for U. S. Navy use. These vehicles require the highest possible energy and power densities and use metallic fuels. Commercial and scientific UUVs do not require these extremely high energy densities, and economy of operation/acquisition costs and ease of turnaround between deployments become the defining requirements.

Silver-zinc batteries (Zn-AgO) may be taken as a benchmark for specific energy for modestly high performance UUVs. This specific energy is normally taken as 100 w-h/kg. The specific energy for the reaction of a typical liquid hydrocarbon fuel with oxygen is approximately 2800 w-h/kg.

If a typical energy conversion system with an efficiency of approximately 25% is used, specific energies on the order of 300-400 w-h/kg, including the mass of the energy conversion system, are possible.

Candidate fuels for such a system include kerosene, jet engine fuel, diesel fuel and their military equivalents. The choice of these fuels does not significantly impact the system. The choice of an oxygen source does. Table I lists several oxygen sources with their oxygen storage densities. This data and chart were provided by Mr. Jonathan A. Peters of ARL Penn State.

Because this effort addresses systems that are suitable for commercial or scientific UUV applications, only readily commercially available and tractable oxygen sources will be further considered. The two sources selected are 3000 psi gaseous oxygen, which is typical of welder's oxygen, and 60% hydrogen peroxide aqueous solution, which is widely used as a bleach in the paper industry. The hydrocarbon selected is JP-5, which is a typical naval jet engine fuel with a flash point suitable for shipboard handling.

Having selected a fuel and oxidizers, the next choice is the type of thermal energy conversion system. The system can be of the external combustion or internal combustion type. An external combustion type is similar to a steam powerplant in which the fuel is burned in a furnace and the heat of combustion is transferred to the steam generator of the closed steam cycle which does the energy conversion. An internal combustion type is similar to a gas turbine powerplant or a turbo-prop aircraft engine in which the hot gaseous products of combustion flow directly to and are the working fluid for the power-producing turbine.

In practice, the bulk of the components required for either the external combustion or internal combustion system are very similar, and the choice of the type will be highly application dependent. Only the internal combustion type will be considered here.

Fig. 1 is a conceptual schematic of an internal combustion system operating on 60% hydrogen peroxide solution; only major components are shown. The gaseous oxygen system would be similar except that the peroxide tank and decomposition chamber are replaced by an oxygen tank and pressure regulator.

TABLE I
Comparison of Oxygen Sources

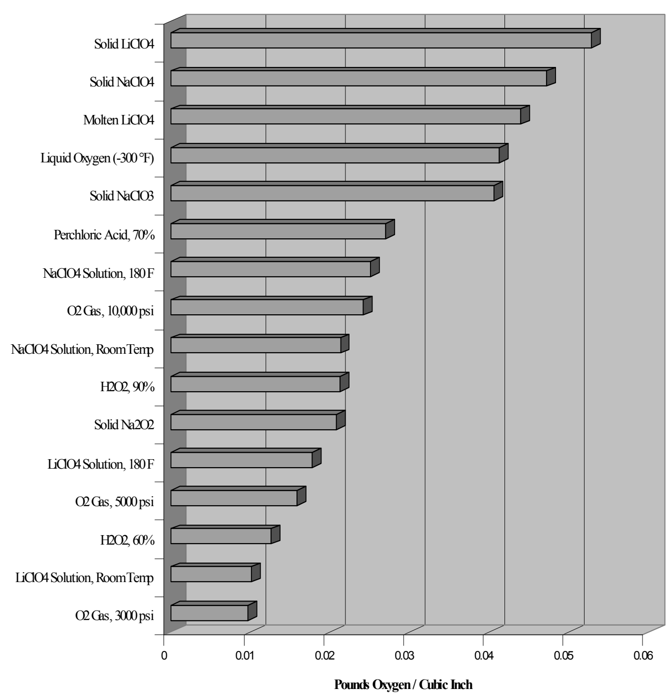

0-7803-7572-6/02/$17.00 © 2002 IEEE.

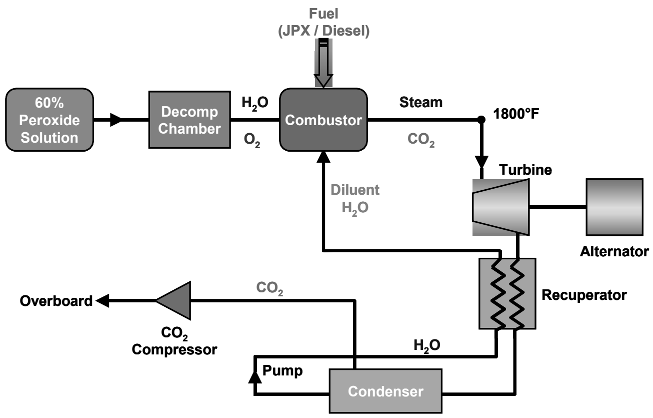

Fig. 1. Hydrocarbon fueled power source.

II. TURBINE AND ALTERNATOR

The schematic shows a turbine prime mover but the choice of a turbine for the low-powered systems (1-3 kW) required for UUVs is not obvious. Fig. 2 shows a group of turbine wheels developed at ARL. The design power levels for these turbine range from a few kilowatts to a megawatt. Until recently, turbines that could operate efficiently at very low power levels were not available. Turbines tend to be very high power devices. They pass a very high flow of working fluid and produce very high power. One approach to producing low power is to take a full admission high power turbine, i.e., a turbine that has nozzles around the full periphery of the wheel and eliminate most of the nozzles to greatly reduce the through-flow and power. Fig. 3 shows the results of such an approach. Note that while the efficiency remains relatively high down to 25-30% admission fraction, it falls off rapidly below that.

The path to high turbine efficiency at low total power is shown in Fig. 4. This figure shows the performance predictions for a family of single-stage axial flow impulse turbines all operating at the same gas supply pressure and temperature and exhaust pressure. Each turbine operates at the same blade speed and has adequate nozzles to produce 2.6 kW/3.5 hp. Note that as the diameter of the turbine is decreased, the rotational speed must increase to provide the constant blade speed. The conclusions are obvious. To achieve an efficiency on the order of 63%, one should operate an approximately one-inch diameter turbine at approximately 450,000 rpm.

Fig. 5 shows the performance as a function of admission fraction for an approximately one-inch diameter turbine wheel operating at 435,000 rpm. Table II shows the design details for this turbine.

Fig. 6 is a photograph of the turbine wheel and nozzle plate. The photo also shows a compressor load impeller, hybrid rolling element bearings and a bearing housing. The impeller was used to load the turbine during dynamometer testing. Fig. 7 shows the turbine wheel mounted in a dynamometer for performance testing.

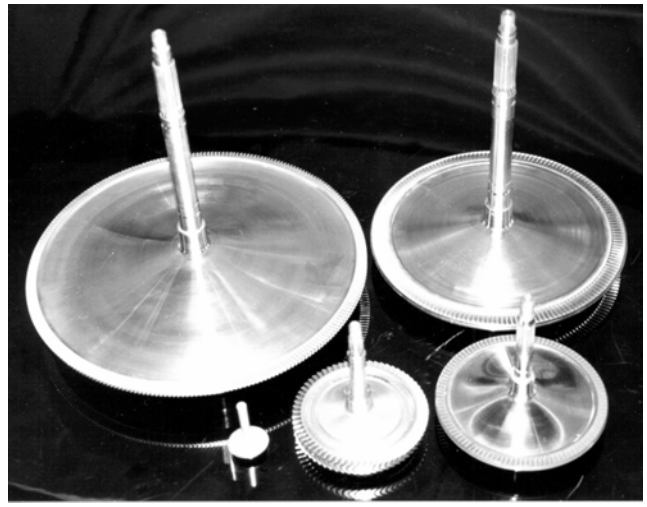

Fig. 2. ARL turbine wheels.

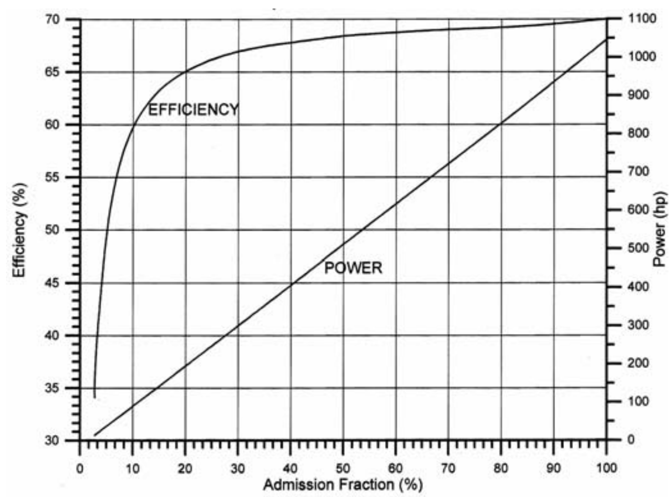

Fig. 3. Results of low power turbine approach.

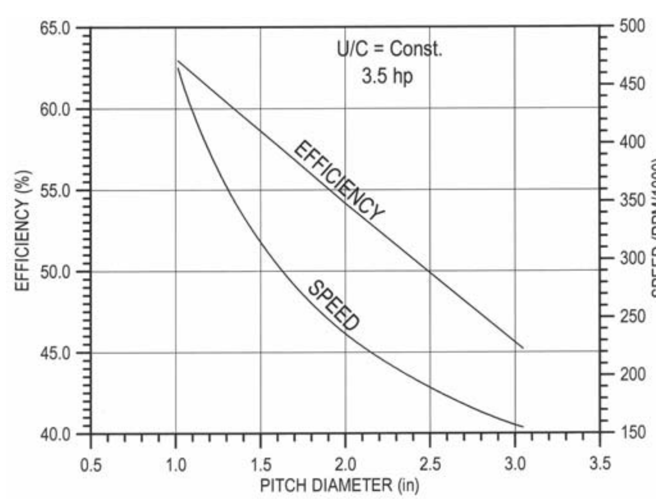

Fig. 4. High efficiency, low power turbine.

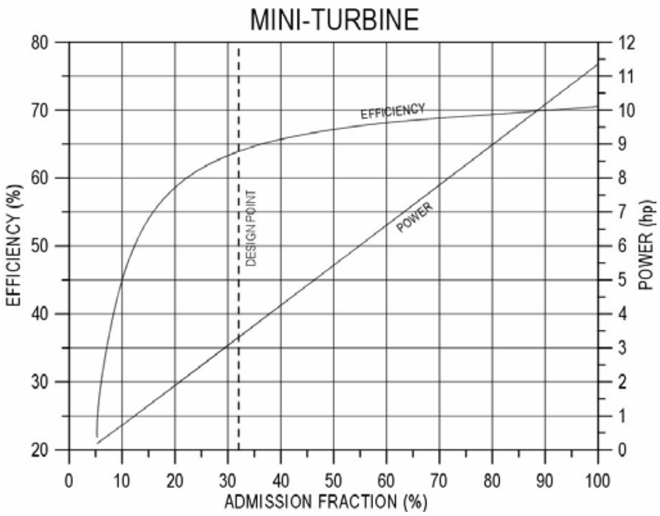

Fig. 5. Performance as a function of admission fraction.

TABLE II
TURBINE DESIGN DETAILS

Pitch diameter (in)	1.014
Number of blades	75
Blade height (in)	0.060
Blade chord (in)	0.074
Inlet angle (°)	25
Exit angle (°)	25
Passage width (in)	0.015
Edge thickness (in)	0.003
Number of nozzles	5
Admission fraction (%)	32
Nozzle throat diameter (in)	0.022
Nozzle exit diameter (in)	0.050
Nozzle angle (°)	15
Design U/C	0.34
Design efficiency (%)	61-63
Design power (hp)	5.0
Design speed (rpm)	435,000

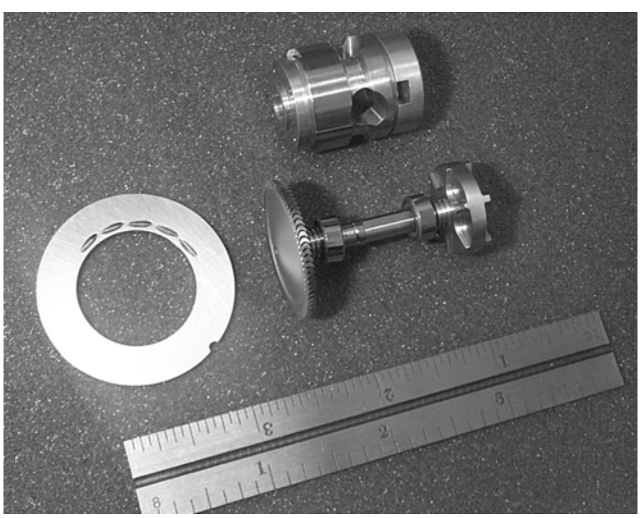

Fig. 6. Turbine wheel and nozzle plate.

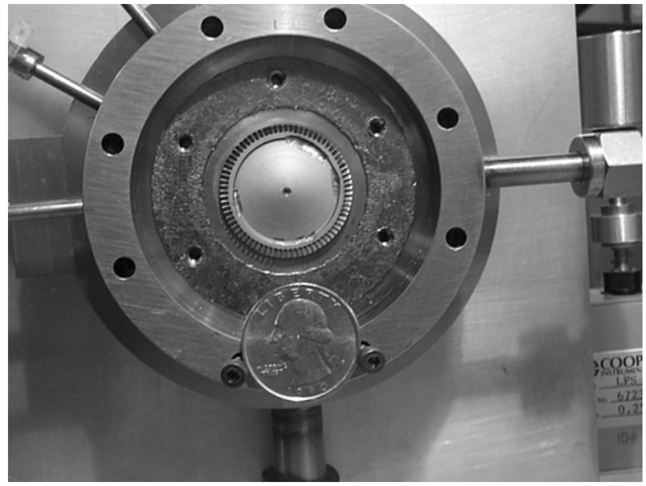

Fig. 7. Turbine in dynamometer.

The turbine wheel was tested on hot and cold carbon dioxide and hot and cold nitrogen. The turbine was generally tested at reduced speed (200,000-300,000 rpm) but at equivalent speed ratio (U/Co). However, the turbine was run at 435,000 rpm for ½ hour. The turbine assembly was fabricated by Barber-Nichols Inc. of Arvada, CO. The tests were conducted at Barber-Nichols under the direction of Mr. Ken Nichols.

Fig. 8 shows test results for the turbine running on hot and cold nitrogen. These tests were run with a shroud on the turbine wheel. The results show good agreement with predictions although the gains expected from the shroud (≈2%) were not fully realized except at the peak speed. It should be noted that the power level was only 1.35 kW and a peak efficiency of 67.2% was measured. This is excellent performance for such a low power.

Fig. 9 shows a drawing of a 3 kW turbo-alternator designed to operate at 435,000 rpm. The turbine is the turbine described above. The alternator was designed for this application by Ashman Technologies of Santa Barbara, CA. Fig. 10 gives some details for the alternator. Fig. 11 gives some specifics for the hybrid bearings for the turbo-alternator. Fig. 12 shows a commercially available high-speed motor/generator that operates at similar speeds.

The turbo-alternator design described here is based on hybrid rolling element bearings. It is anticipated that final versions of the systems would use gas lubricated foil bearings which would have almost unlimited life.

III. CARBON DIOXIDE PUMPING

One disadvantage of the internal combustion type of energy conversion system is that the carbon dioxide in the turbine exhaust must be pumped overboard. Fortunately, CO_2 is reasonably soluble in water. Fig. 13 shows the solubility as a function of pressure and temperature. The approach used is to take in seawater through a vane motor,

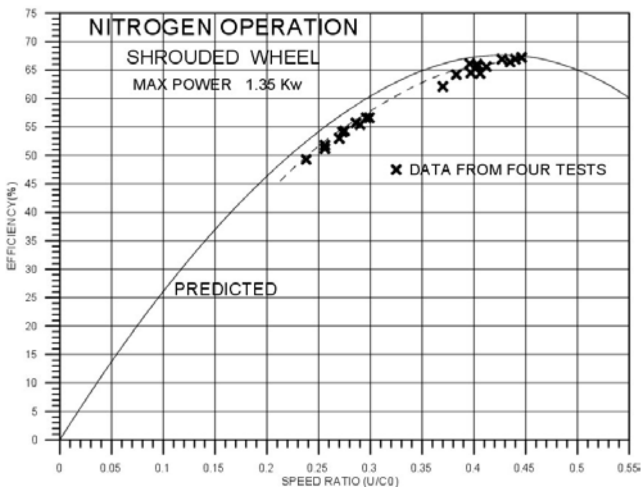

Fig. 8. Results for turbine running on hot and cold nitrogen.

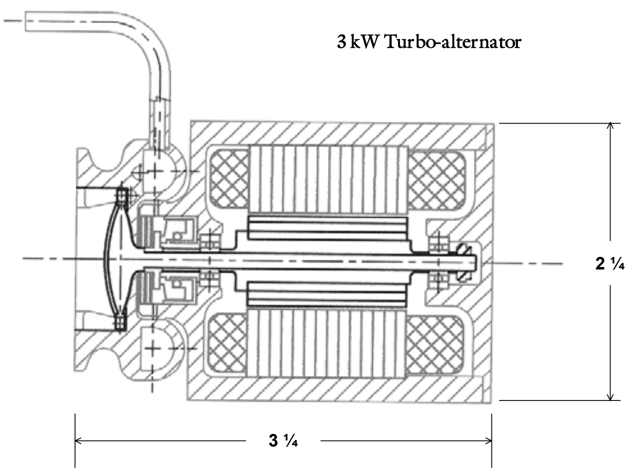

Fig. 9. 3 kW turbo-alternator.

Alternator Description	
ROTOR	Nd-Fe-B
Length (in)	1.24
Magnet Dia. (in)	0.61
Rotor Dia. (in)	0.71
Rotor Mass (lbm)	0.10
STATOR	
I.D. (in)	0.77
Physical Air Gap (in)	0.03
Magnetic Air Gap (in)	0.08
Length-Over Turns (in)	1.89
Lamination O.D. (in)	1.82
Alternator Operation (400,000 Rpm)	
Poles x Slots	4 x 6
No-Load Voltage	127.2 V L-N 220.3 V L-L
Full Load Power (kW)	3.15 @ 1.0 PF
Full Load Voltage (V)	200 RMS L-L
Full Load Current (A)	9.31 / Phase

Fig. 10. Turbo-alternator description.

Rolling Element Bearings	
Bearing	Barden R2B
Type	Angular Contact / Ceramic Hybrid
O.D.	0.375 in.
Bore	0.125 in.
Length	0.156 in.
No. of Balls	7
Ball Diameter	0.0625 in.
Raceways	SAE 52100 Steel
Balls	Silicon Nitride
Separator	Phenolic
Life at 425,000 RPM	
Ganged Nozzles (3.0 lbf)	B_{10} = 300 - 400 hrs
Separated Nozzles (1.5 lbf)	B_{10} = 600 - 800 hrs

Fig. 11. Turbo-alternator hybrid bearings.

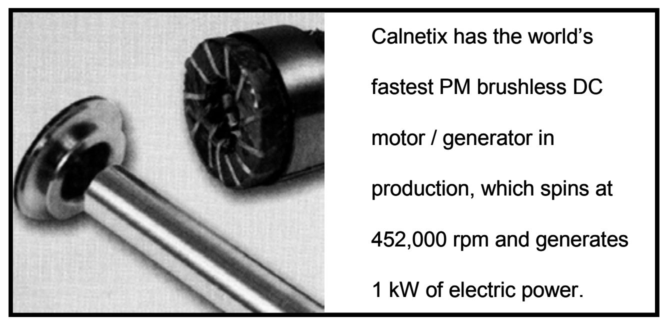

Fig. 12. Commercial high-speed motor/generator.

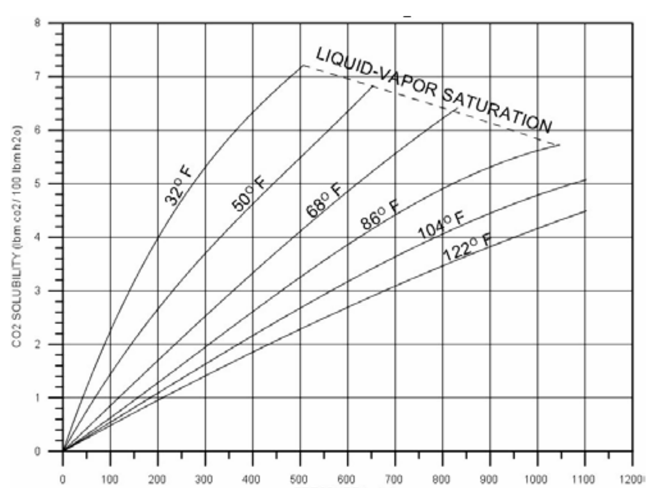

Fig. 13. Solubility of CO_2 in water.

mix the CO_2 and the seawater and then pump the mixture overboard. The mixing cools the CO_2 to very close to seawater temperature, which reduces work of compression and increases the solubility. To some extent, the CO_2 will dissolve in the seawater during the compression. At a minimum, an isothermal compression, which minimizes the work of compression, is closely approximated. The output power of the seawater vane motor is used to help drive the vane pump/compressor. A small centrifugal or scroll compressor may be used to supercharge the vane pump.

Tests at the Applied Research Laboratory have shown that the carbon dioxide may be pumped overboard using commercially available vane pumps and water. The tests were configured to allow a variety of pump speeds, pump inlet pressures and backpressures. Fig. 14 shows the test schematic with a regulated CO_2 supply and carefully measured gas and water flow rates. The pump, which was not altered for the carbon dioxide pumping tests, was a Vickers model PF4 with carbon vanes and stainless steel moving parts, manufactured by Vickers, Inc., of Jackson, MS. Its displacement is 1.15 in^3/rev; its design shaft speed is 5000 rpm, and its design flow rate is 21 gpm at a backpressure of 1425 psia. Fig. 15 shows a photograph of the test setup. The vane pump is visible at the middle-left side of the photo, to the left of the pressure gauge.

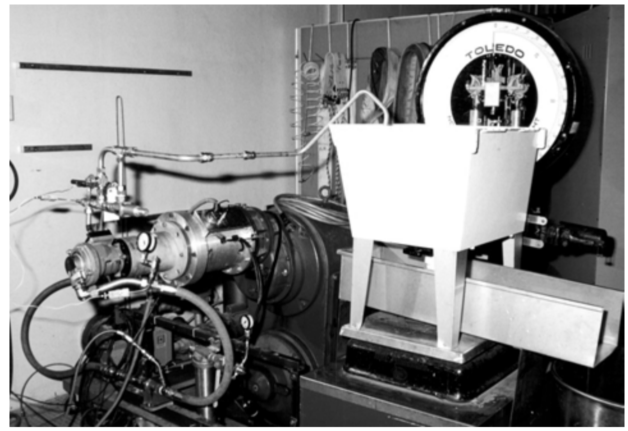

Fig. 15. Test setup for carbon dioxide pumping tests in which carbon dioxide was pumped to back pressures simulating moderate ocean depths.

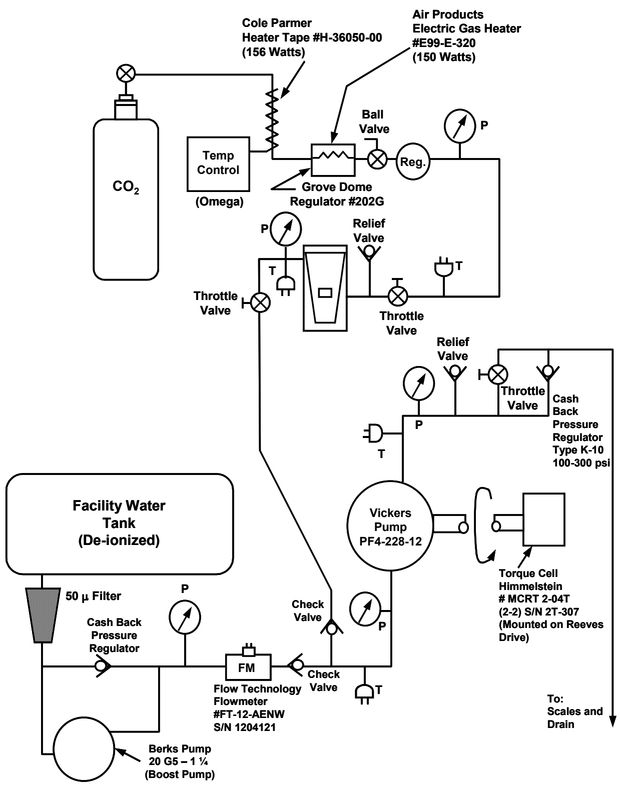

Fig. 14. Test schematic diagram for carbon dioxide pumping tests at ARL Penn State.

Results showed that the carbon dioxide was partially dissolved in the water stream and that the remaining CO_2 was compressed nearly isothermally to the exit pressure. Testing showed that a moderate increase in inlet pressure above the 15 psia design inlet pressure for the pump eliminated cavitation and the relatively low CO_2 mass flow that resulted from the cavitation. Fig. 16 shows the CO_2 pumping performance was improved when a moderate inlet pressure of 35 psig was set at the inlet of the pump. The amount of CO_2 actually dissolved did not approach the theoretical limit at the exit pressure, but the total amount compressed was approximately 60% of that theoretical limit (1.25 lbm CO_2/100 lbm water at 68°F, 150 psig). The mass of carbon dioxide pumped at the higher backpressure of 300 psig was a lower percentage of the dissolution limit at that pressure (probably due to leakage around the tips of the carbon vanes and re-expansion of the clearance volume), but the tests did demonstrate the ability to operate at that more severe condition. This means that the total amount of water should be approximately twice that theoretically required to dissolve the CO_2. The vane pump should also have a minimum clearance volume.

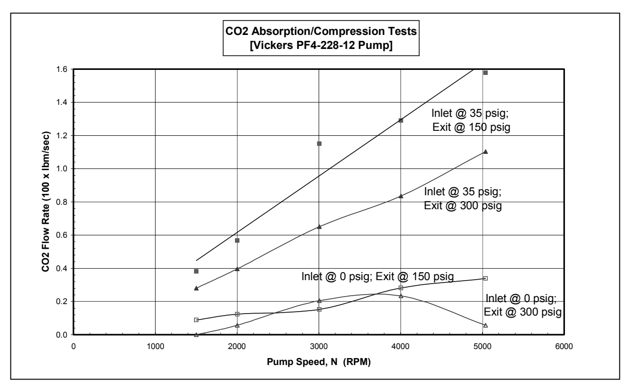

Fig. 16. Test data show that carbon dioxide flow rate pumped overboard with a commercial vane pump could exceed the solubility limit of the carbon dioxide in water through a combination of compression and dissolution.

Later testing at ARL Penn State identified an efficient means of compressing the carbon dioxide products of combustion to pressures higher than the 35 psig inlet pressures noted in Fig. 16.

It should be noted that the power to exhaust the CO_2 is not a large fraction of the turbine output; it is typically less than 10% and is far less than the additional power gained from the low turbine exhaust pressure. It should also be noted that at say 60°F the CO_2 will liquefy at approximately 720 psia, which corresponds to a depth of approximately 1600 ft. The work of compression does not significantly increase for deeper depths.

IV. System Performance

For the gaseous oxygen system, the amount of residual oxygen is determined by the lowest oxygen tank pressure that can support full power operation unless water back-fill is used. In order to minimize the residual or unusable oxygen, the combustor and nominal turbine inlet pressure for both systems is taken as 300 psia.

Referring to the schematic diagram of Fig. 1, it is seen that diluent water is added to the combustor to maintain an 1800°F turbine inlet temperature. The turbine working fluid is nominally a mixture of 85% steam and 15% carbon dioxide.

The steam in the turbine exhaust is condensed to liquid in a condenser which will be maintained at 5 psia by the use of a small vacuum pump if necessary. Table III shows significant parameters for both systems for an application that will provide 2 kW for 25 hours. This application grew out of discussions of power and energy requirements with a commercial UUV operator.

Fig. 17 is a layout of the peroxide-based system. Additional parameters are shown in Table IV. The system specific energy is 300.0 w-h/kg and the system energy density is 261.4 w-h/L. The system section is 21.8 lbf positively buoyant.

Fig. 18 is a layout of the gaseous oxygen system. Additional parameters are shown in Table V. The system specific energy is 464.3 w-h/kg and the system energy density is 162.2 w-h/L. The system section is 389 lbf positively buoyant.

TABLE III
Design Parameters

	H_2O_2	GOx
Electric power out (kW)	2	2
Turbine inlet pressure (psia)	300	300
Turbine exhaust pressure (psia)	5	5
Turbine inlet temperature (°F)	1800	1800
Turbine efficiency (%)	63	63
Recuperator effectiveness (%)	85	85
CO_2 compressor efficiency (%)	50	50
Fuel flow (lbm/hr)	0.953	1.317
Peroxide solution flow (lbm/hr)	11.46	—
Oxygen flow (lbm/hr)	—	4.472
Mass fraction CO_2 in exhaust (%)	16.0	21.2
Thermal system energy conversion efficiency (%)	27.6	29.4
Overall energy conversion efficiency (%)	26.2	27.9

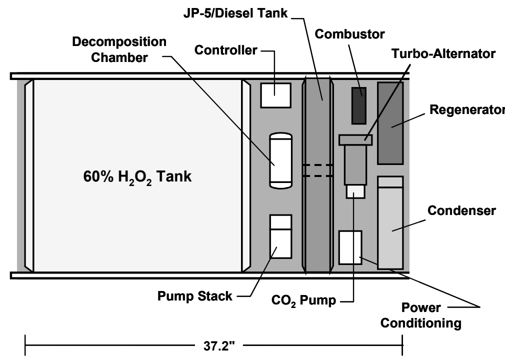

Fig. 17. 21-inch diameter hydrogen peroxide-based system, 2 kW for 25 hrs.

TABLE IV

Length of solution tank (in)	21.3
Length of fuel tank (in)	2.9
Length of machinery section (in)	6.0
Length of ancillary section (in)	5.0
Length of clearance space (in)	2.0
Total	37.2

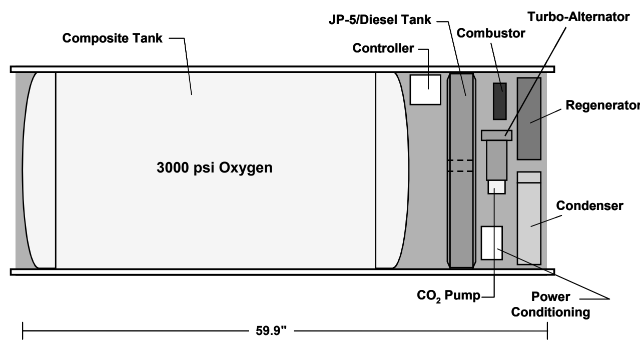

Fig. 18. 21-inch diameter gaseous oxygen system, 2 kW for 25 hrs.

TABLE V

Length of oxygen tank [torispherical ends] (in)	43.0
Length of fuel tank (in)	3.9
Length of machinery section (in)	6.0
Length of ancillary section (in)	5.0
Length of clearance space (in)	2.0
Total	59.9

V. Off-Design Performance

Batteries are usually more efficient at reduced load. The opposite is often true for thermal systems. Fig. 19 shows the turbine efficiency and overall system efficiency as a function of load. Note that the abscissa is a reversed scale. These curves are fairly flat except at very low power. This is a result of the turbine running at a constant speed to maintain constant alternator voltage. The turbine output power is reduced by lowering the turbine supply pressure. This lowers the mass flow through the turbine and, as a result, the condenser pressure is reduced. The turbine nozzles thus tend to operate at a constant pressure ratio and maintain their efficiency. Parasitic bearing and seal losses eventually reduce the turbine efficiency.

The system efficiency tends to decrease less than the turbine efficiency because the higher turbine exhaust temperature increases the heat transfer in the recuperator which somewhat offsets the loss in turbine efficiency.

VI. Operation at Depth

These systems are semi-closed and discharge water and carbon dioxide. The work to pump the CO_2 overboard increases with depth, which decreases the energy conversion efficiency. This work is not a large fraction of the turbine output and the loss of performance with depth is not severe. Fig. 20 shows the falloff of energy conversion efficiency with depth of operation.

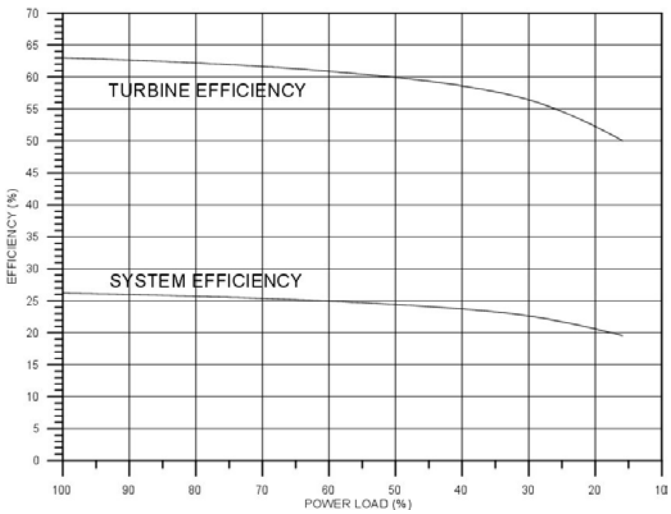

Fig. 19. Turbine efficiency and overall system efficiency as a function of load.

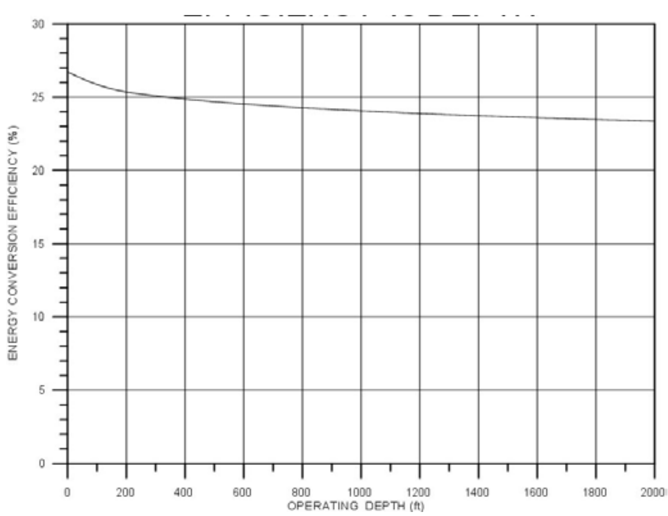

Fig. 20. Energy conversion efficiency as a function of operating depth.

VII. Performance versus Total Energy

A battery produces electric power directly. The thermal systems require an energy conversion system including an alternator. At very low total energy, the conversion system will dominate both the size and weight of the system and the specific energy and energy density will be low. As the total energy increases, the conversion system volume and weight become less important and the system specific energy and energy density approach that of the reactants alone. This is shown for the peroxide-based system in Fig. 21 and for the oxygen-based system in Fig. 22.

VIII. Power Section Length

Fig. 23 is a plot of the normalized length of the power and energy sections for the two-kilowatt systems in 21-inch diameter UUVs. Several things should be noted. The system has finite length (13 inches in this case) even for zero total energy produced. This is essentially the length of the energy conversion equipment. A very generous length has been allotted to be conservative and to allow for contingencies. This length can probably be reduced in a well packaged system. The low energy portions of the curves are non-linear because of the end effects of the fuel and oxidizer storage tanks.

There is a change in slope of the peroxide system curve at about 62 kW-hr. A UUV power section should be positively or at least neutrally buoyant. Because of the generous space allowance for the energy conversion equipment, the peroxide system is positively buoyant up to this total energy. At greater energies, additional space to achieve neutral buoyancy must be allocated, which increases the section length at a greater rate. The system energy density calculations do not include the additional space. The oxygen system is always highly positively buoyant.

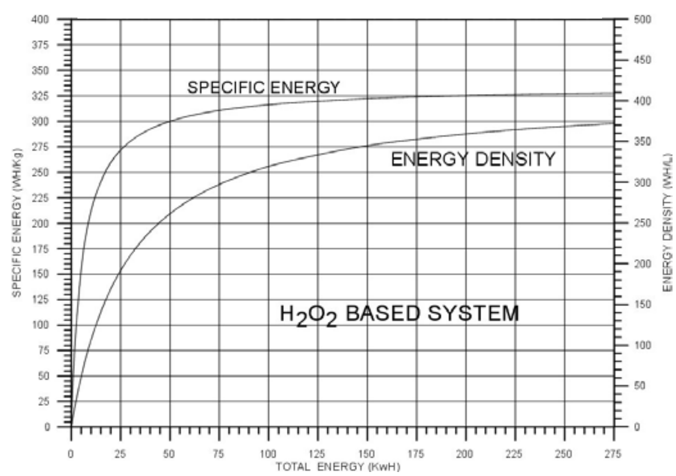

Fig. 21. Performance versus total energy for peroxide-based system.

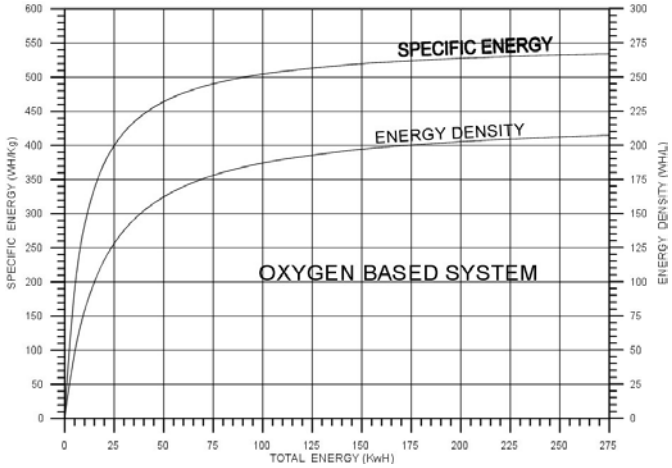

Fig. 22. Performance versus total energy for oxygen-based system.

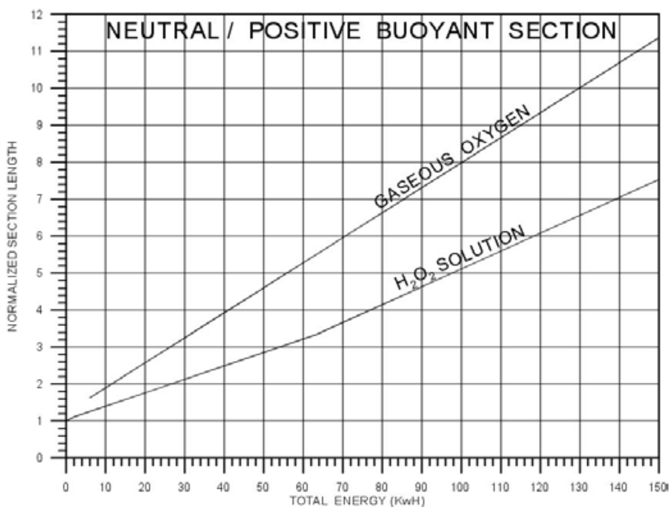

Fig. 23. Normalized power section length for 2 kW UUV systems.

IX. Ease of Turnaround

These systems may be regarded as "gas-and-go" systems. There is no inherent reason why anything more than a refilling of the oxidizer and fuel tanks should be required between runs.

X. Conclusions

The systems described above attain specific energies of 300 and 464 w-h/kg and energy densities of 261 and 162 w-hr/L, respectively. Significant improvements are possible through more compact energy conversion and ancillary component packaging. The fuels and oxidizer used are readily available commercial commodities. The systems are capable of rapid turnaround by refilling their tanks. The size and energy density of the gaseous oxygen system can be improved significantly by increasing the oxygen storage pressure. The buoyancy of the oxygen system may be used to offset the weight of other vehicle sections.

Acknowledgement

This work was partially supported by the Office of Naval Research under the cognizance of Dr. Richard T. Carlin.